Forecasting and Detection of Fatigue Cracks in Polycrystalline Alloys With Ultrasonic Testing Via Discrete Wavelet Transform

Hassan Alqahtani[1]
Department of Mechanical Engineering,
Pennsylvania State University,
University Park, PA 16802;
Department of Mechanical Engineering,
Taibah University,
Medina 42353, Saudi Arabia
e-mail: hhq1408@gmail.com

Asok Ray
Fellow ASME
Departments of Mechanical Engineering and Mathematics,
Pennsylvania State University,
University Park, PA 16802
e-mail: axr2@psu.edu

Forecasting and detection of fatigue cracks play a key role in damage mitigation of mechanical structures (e.g., those made of polycrystalline alloys) to enhance their service life, and ultrasonic testing (UT) has emerged as a powerful tool for detection of fatigue cracks at early stages of damage evolution. Along this line, the work reported in this paper aims to improve the performance of fatigue crack forecasting and detection based on a synergistic combination of discrete wavelet transform (DWT) and Hilbert transform (HT) of UT data, collected from a computer-instrumented and computer-controlled fatigue-testing apparatus. Performance of the proposed method is evaluated by comparison with the images generated from a digital microscope, which are treated as the ground truth in this paper. The results of comparison reveal that forthcoming fatigue cracks can be detected ahead of their appearance on the surface of test specimens. The proposed method apparently outperforms both HT and conventional DWT, when they are applied individually, because the synergistic combination of DWT and HT provides a better characterization of UT signal attenuation for detection of fatigue crack damage. [DOI: 10.1115/1.4049732]

Keywords: failure analysis, fault analysis

1 Introduction

Fabrication is a critical ingredient in the production of mechanical machinery, which are often subjected to flaws in manufactured components. When a machinery is in operation, the flaw size in its individual component(s) may keep on growing due to the fatigue stresses resulting from repetitive loading; once a flaw reaches the critical size, the component fracture begins to take place [1–5]. Hence, these flaws are considered to be the root cause of structural degradation.

In many instances of mechanical failures, damage precursors (e.g., dislocations and voids) would evolve inside the component structure, followed by their indicators (e.g., cracks) before a failure actually occurs. Since such indicators may not be observable at an early stage of damage (e.g., cracks less than 0.25 mm), fatigue damage monitoring is necessary to forecast the damage before these indicators appear; this is specifically true for components that may have grave consequences on the human life, the economy, and the environment.

Important roles of real-time sensing of damage include continuous inspection of mechanical structures and updated measurements of product quality so that their reliability can be assessed and the protection against unexpected failures is maintained. Health monitoring of mechanical structures using visual testing (VT) is a widely used method of inspection in industrial applications, by which many macroscopic flaws (e.g., surface deformation/crack, poor welding, and improper surface finish) can be detected. However, VT has two significant disadvantages:

(1) *Limitations regarding flaw detection*: Examples include detection of micro-scale and meso-scale flaws on surfaces and internal defects (e.g., voids and inclusions) of the structure.
(2) *Intermittent inspection*: The damage could occur in-between two inspection events.

Therefore, real-time sensing of damage with computer-assisted analytical methods of nondestructive testing (NDT) is considered to be essential in a majority of industrial applications.

Ultrasonic testing (UT) [6,7] is an NDT method that is widely used to estimate the internal damage and defects of mechanical structures. The operating frequencies in UT sensors may range normally between 400 kHz and 25 MHz, which exceed the human audible range which is between 16 Hz and 20 kHz [8]. The frequencies of UT play a major role in determining the internal defects. For example, high frequencies (e.g., 15 MHz) that are used for contact testing applications have two advantages. First, due to the sensitivity at ~5 MHz, UT can detect small material imperfections (i.e., discontinuities). Second, due to the high resolution at ~5 MHz, UT sensors can determine the location of discontinuities, even if these discontinuities are very closely spaced. However, high frequencies may not be able to detect discontinuities of some components that have large grain structures (e.g., castings) because these high-frequency (e.g., ~5 MHz and higher) signals are significantly attenuated while passing through a coarse-grained material. On the other hand, an advantage of low-frequency (e.g., ~1 MHz and less) signals is that they perform well for testing coarse-grained materials; however, their sensitivity and resolution are usually inadequate [9].

Transducers, which are one of the functional units of UT sensors, belong to two broad classes of usage: (i) transmitter transducers and (ii) receiver transducers. The transmitter transducer converts electrical energy into mechanical energy in the form of ultrasonic waves, while the receiver transducer converts the mechanical vibrations of ultrasonic waves into electrical signals. The basic principle and functionalities of crack detection using UT are as follows:

> *The ultrasonic energy, generated by the transmitter transducer, which has known and fixed characteristics, propagates through the medium of the structure and a part of this energy is reflected back to the transmitter transducer; the remaining part of the energy is attenuated (and possibly distorted) before reaching the receiver transducer. The resulting attenuation and distortion (e.g., due to a damage precursor) in the received waveform is used for damage assessment in the structure. In this way, UT characterizes material conditions and locates the material flaws that could eventually lead to a structural failure [7,10–12].*

[1]Corresponding author.

Manuscript received September 29, 2020; final manuscript received December 22, 2020; published online February 23, 2021. Assoc. Editor: Ed Habtour.

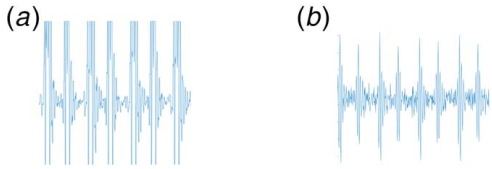

Fig. 1 Typical ultrasonic signals at the receiver end: (*a*) Crack-free specimen and (*b*) cracked specimen

The tools of both VT and UT have been used in the work reported in this paper to forecast and detect the onset of fatigue cracks at the notch tip of specimens on a laboratory apparatus. The most important aspect of this investigation is to improve the performance of the monitoring system for forecasting and detection of fatigue crack damage. The digital microscope in the test apparatus supports the VT observations by magnifying the notch tip images, which are used in conjunction with UT data. Generally, spurious signals (e.g., vibrations) from the surrounding environment of the laboratory generate various types of disturbances and noise, which degrades the quality of UT signals; therefore, the disturbance and noise contamination need to be filtered out from the UT signals.

This paper evaluates the performance of a UT-based procedure of damage forecasting and detection by comparison with the results of VT images that are taken to be the ground truth in this paper. The time-domain observations on the laboratory apparatus reveal that the attenuation of a UT signal can be consistently detected before any meaningful information is available from the VT images; otherwise, the UT detection may not have much use. Therefore, it is necessary to observe the main features of the UT signal (e.g., the texture of UT signals and profiles of the signal energy). Figure 1(*a*) displays the profile of the received UT signal on a typical crack-free specimen, while Fig. 1(*b*) shows the same for a typical fatigue cracked specimen.

The paper is organized in six sections including the current section. Section 2 describes the laboratory apparatus on which experiments have been conducted to validate the theoretical part of the work reported in this paper. Section 3 provides the necessary background on signal processing for UT-based fatigue crack forecasting and detection of fatigue cracks. It also presents the mathematical concepts of discrete wavelet transform (DWT), Hilbert transform (HT), and the proposed DWT and HT-based methods. Section 4 compares the results of experimentation via DWT, HT, and the proposed method by making use of VT images. Section 5 presents and discusses the results of experimentation on the typical test specimens. Section 6 summarizes and concludes the paper along with recommendations for future research.

2 Description of the Experimental Apparatus

Figure 2(*a*) presents the experimental apparatus that is built upon a computer-controlled and computer-instrumented fatigue-testing machine (MTS®, Berlin, NJ), which is equipped with a digital microscope for VT and ultrasonic sensors (OLYMPUS®, Shinjuku, Tokyo, Japan) for UT. The UT transducers are excited by 15 MHz ultrasonic waves, injected to the specimens by a piezoelectric transducer, called the transmitter, and the transmitted signals are detected by another piezoelectric transducer, called the receiver, that is located on the other side of the notch tip, as seen in Fig. 2(*a*). When the crack begins to propagate, the UT signal starts to attenuate, because a part of the signal is reflected and thus the full signal is not received by the receiver. Moreover, the digital microscope is synchronized with the UT to monitor the crack behavior and to provide the evidence for attenuation of the UT signal. The digital microscope is located close to the notch tip since the crack appearance starts at the crack tip due to the high-stress concentration.

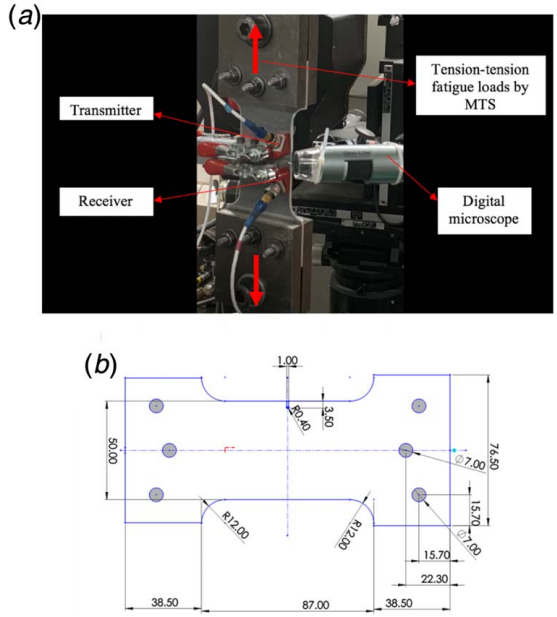

Fig. 2 The fatigue-testing apparatus and ancillaries: (*a*) Picture of the experimental apparatus and (*b*) computer-aided design (CAD) drawing of an AL7075-T6 aluminum alloy specimen (all dimensions are in *millimeter* and are not to scale)

In the reported work, experiments have been conducted with *three* identical[2] test specimens (that are made of AL7075-T6 aluminum alloy) to investigate the fatigue damage properties of polycrystalline materials. The dimensions of these specimens are 3 mm thickness and 50 mm width. A (1–3.5 mm) U-notch is incorporated at the edge, as seen in Fig. 2(*b*) that shows the CAD drawing of a typical test specimen. In the experiments that are used to forecast and detect the onset of fatigue cracks, all specimens are subjected to tension-tension load cycles, and the loads are generated by the fatigue-testing machine (see Fig. 2(*a*)). A typical target set-point is the tensile-tensile load fluctuation with (peak) 11,000 N and (valley) 3000 N (i.e., the load range is 8000 N).

3 Background: Signal Processing for Ultrasonic Testing-Based Fatigue Crack Detection

In the discipline of signal processing, mathematical transformations are used to extract pertinent information, which is embedded in the time series of the raw signal. However, in many cases, the time-domain analysis of a signal may not be the best way for anomaly detection, because the most relevant signal information can be conveniently extracted from the frequency spectrum. The Fourier transform (FT) is commonly used for conversion of time-domain signals to the frequency domain. However, usage of FT may not be suitable for non-stationary signals, where localization of both time and frequency is necessary. For non-stationary signals, a modified version of FT, called the short time Fourier transform (STFT), could be used if the signal can be split into segments, where the signal of each segment is assumed to be stationary [13].

The wavelet transform (WT) largely overcomes the localization problems of FT and STFT [13,14], because WT provides both

[2]The rationale for using three (apparently) identical specimens is to establish the consistency of experimental results. It is noted that the fatigue life of identical test specimens may significantly vary due to uncertainties resulting from internal defects as well as from the machining process.

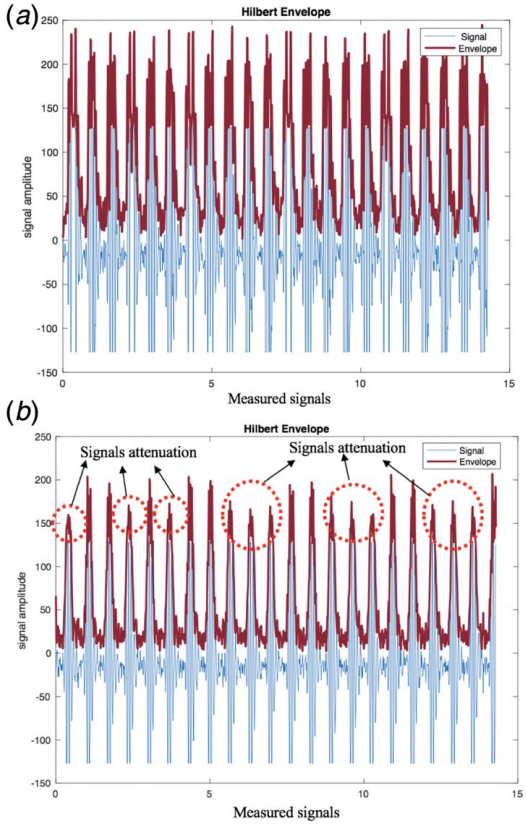

Fig. 3 Envelope detection of UT signals for typical crack-free and cracked specimens, where the abscissa is the measured UT signal and the ordinate is signal amplitude: (*a*) UT signals response for a crack-free specimen and (*b*) UT signals response for a cracked specimen

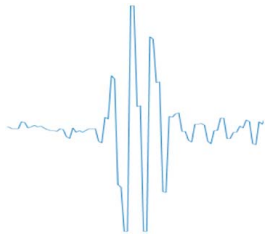

Fig. 4 The waveform of a typical UT signal

time and frequency localization at different scales and time-translation and provides better time-frequency representation for the signal. However, according to Heisenberg uncertainty principle, the windows of time and frequency localization cannot be made arbitrarily small. The fundamental operation using WT is signal decomposition, where the original signal is passed through a bank of high-pass and low-pass filters, where the output of a low-pass filter is further orthogonally decomposed into two parts, namely, low frequencies and high frequencies. This procedure is repeated until the signal is decomposed to the desired level. The final step is to determine the frequency band to which the signal is physically relevant.

In this paper, the most important information derived from UT signals is the data set found before the fatigue crack takes place, and this vital information of UT data is obtained by applying two methods. The first method is a DWT, called multiresolution analysis (MRA), which decomposes a generated UT signal into the detail and approximation of the signal [13]. The detail represents high-frequency components of the signal, while the approximation represents the low-frequency components of the signal. The multilevel signal decomposition is the fundamental process of MRA, where each approximation portion of the signal is decomposed into a hierarchical set of details and approximations. In this investigation, the

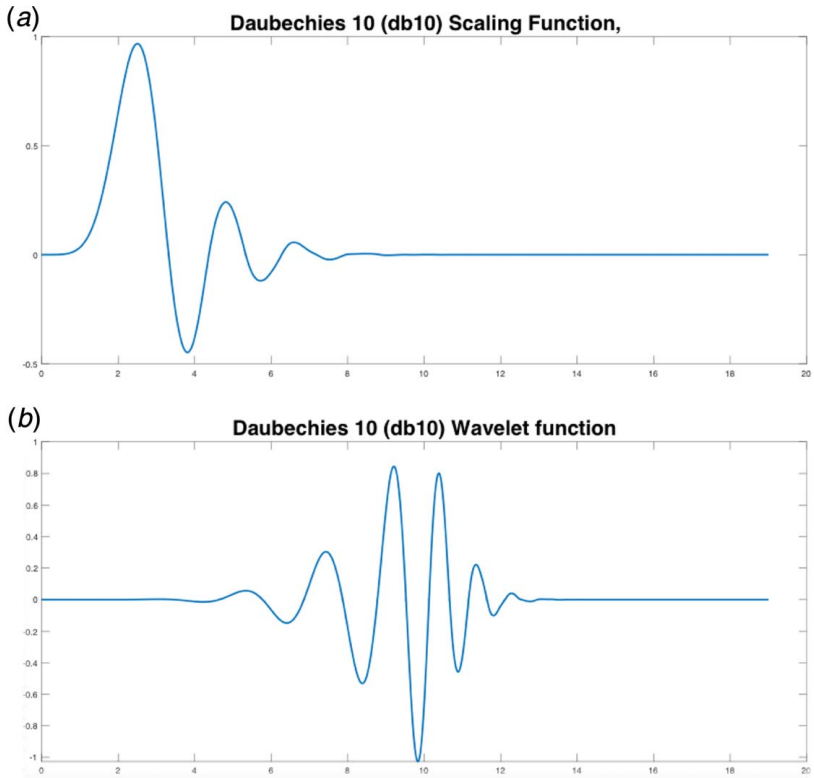

Fig. 5 Scaling and wavelet functions for db10: (*a*) scaling function (ϕ) and (*b*) wavelet function (ψ)

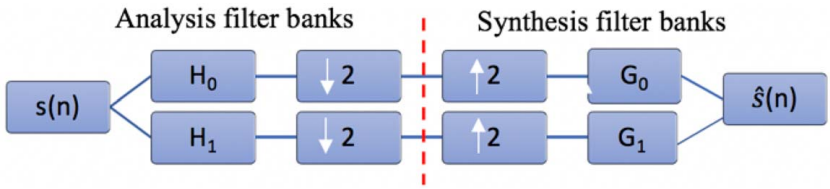

Fig. 6 Two-channel analysis and synthesis filter banks in MRA

preferred wavelet decomposition level that provides the best detection of the crack onset is a fourth level wavelet decomposition.

Another method of signal processing is envelope detection via the HT [15]. In many engineering applications (e.g., vibration, rolling element bearings, and gearboxes), the envelope detection method is one of the main techniques that are used for fault diagnosis. Thus, HT has become one of the methods that are widely used for analysis of non-stationary signals, where relevant information (e.g., amplitude, instantaneous phase, and frequency) of signals can be extracted by using HT [15,16].

The principle of HT-based envelope detection is built upon the (complex-valued) analytical signal, generated from the input data. The real part of the analytical signal is the original signal, while the imaginary part is HT of the original signal. Furthermore, the signal envelope characterizes the upper and lower boundaries of the signal. In other words, it can illustrate the behavior of the signal in the time-domain. In this paper, UT signals contain a rapidly oscillating component which is measured in time-domain, as seen in Figs. 3(*a*) and 3(*b*) that represent the widely different signal attenuation of crack-free specimens and fatigue cracked specimens, respectively, and the attenuation of UT signals becomes more obvious using HT. Therefore, the (HT-based) envelope detection technique has been used to detect the transition between crack-free specimens and cracked specimens [17–19].

This paper develops and experimentally validates a novel method of forecasting and detection of fatigue cracks in polycrystalline alloys by combining the envelope detection property of HT with DWT analysis of UT signals. The objective here is to enhance the forecasting and detection of fatigue crack onset. The proposed method relies on the energy of the signal envelope that is significantly influenced by fatigue crack initiation, where a part of the signal is reflected due to the structural damage of the specimen. Consequently, the energy of the signal envelope is attenuated at the onset of fatigue crack. Then, the energy profile envelope of the receiver signal is analyzed by DWT; the rationale is that DWT is capable of extracting the relevant information both locally and globally.

In the above context, major contributions of the current paper are briefly summarized as follows:

- *Performance enhancement of real-time health monitoring*: Measurements of UT data, in combination with images of VT from a digital microscope, yields significantly better detection of the onset of a fatigue crack.
- *Time-frequency analysis of UT data*: A synergistic combination of HT and DWT has been implemented and demonstrated on UT signals for forecasting and detection of fatigue cracks.

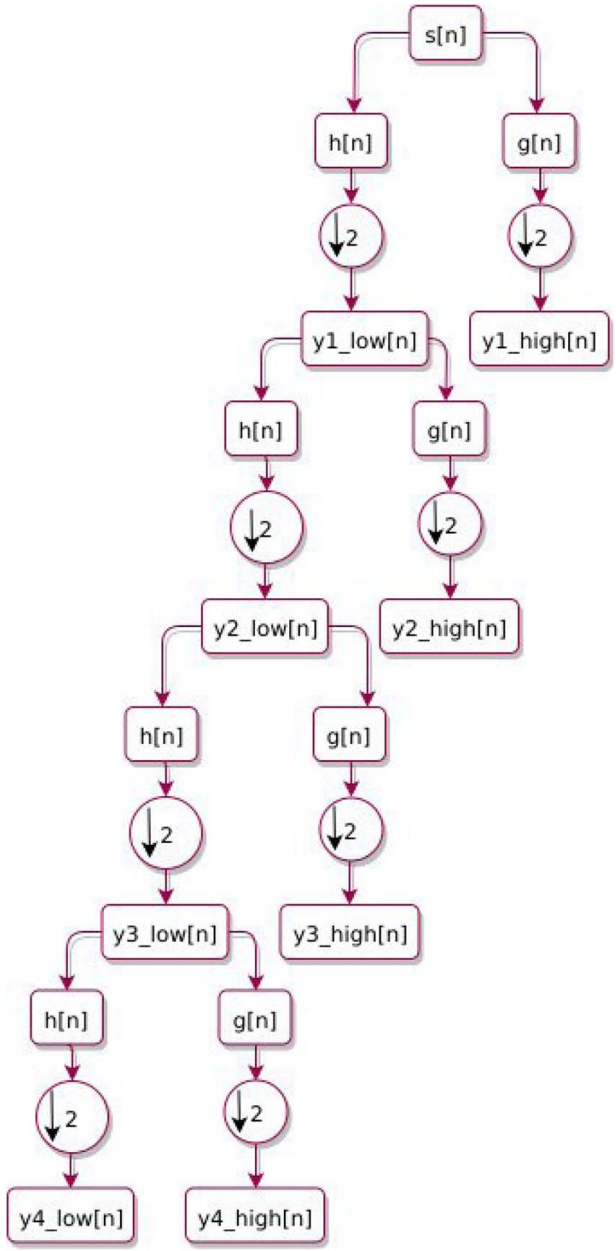

Fig. 7 A four-level dyadic representation of the DWT of ultrasonic signals using a two-channel filter bank

4 Methodologies and Procedures

This section presents the details of methodologies and procedures for forecasting and detection of fatigue crack damage, which involve DWT and HT as well as their combination.

4.1 The Discrete Wavelet Transform. It is well known that a DWT procedure can be conveniently constructed based on the principle of MRA [13], where the signals are analyzed at different scales and time translations. The general concept of MRA was originally developed by Mallat [14] in 1988 and, in the same year, Daubechies [20] defined a technique to build compact-support orthogonal wavelets. In this paper, the Daubechies wavelet basis function, db10, is applied for decomposition of the multilevel wavelet signal. The rationale for applying db10 is that the mother wavelet function of db10 is largely similar to the original signal [21,22], as seen in Figs. 4 and 5(*b*).

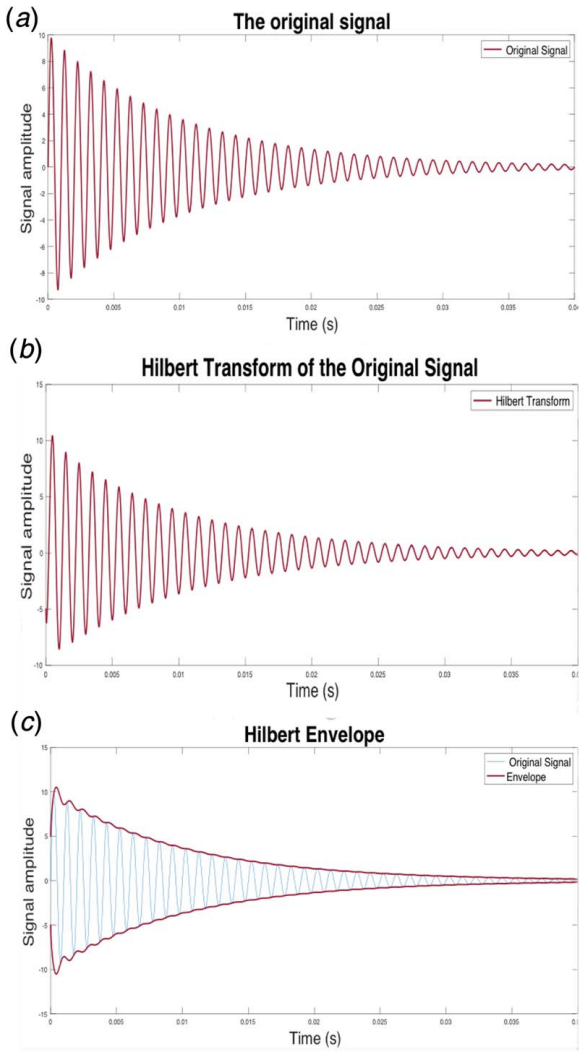

Fig. 8 An illustration of the concept of envelope detection: (*a*) original signal, (*b*) HT signal, and (c) signal envelope

In MRA, the "detailed" components of a signal are extracted by a bank of high-pass filters, and the "averaged"(also called "approximate") components of the signal are extracted by a bank of low-pass filters. These two operations have significant roles toward determining the resolution of the signal. The first operation is the signal filtering, which represents a high-pass filter and a low-pass filter. The second operation is the signal scaling, where the scale of the signal is changed by down-sampling and up-sampling operations [13].

MRA has two main stages, as seen in Fig. 6, where the first stage is the analysis filter bank. In this stage, the input signal of each level passes through two steps. The first step is the signal filtering, where the signal passes through a low-pass or high-pass filter. The second step is the signal down-sampling, where some of the signal samples are excluded. For example, down-sampling the signal by two, that is, removing every other sample of the signal, and it is widely used in the first stage of DWT. The approximation signal denotes the output of the low-pass filter after the down-sampling operation, and the detail signal represents the output of the high-pass filter after the down-sampling operation. For the most part, the approximation signal at each level is considered to be the input signal for the next level [23,24]. The signal analysis procedure of the first stage (i.e., analysis filter bank), illustrated in Fig. 7, is described as follows:

(1) The UT signal passes through half-band (low-pass and high-pass) digital filters, where the signal is convolved with impulse response $h[n]$ and $g[n]$, respectively. The half-band low-pass filter eliminates frequencies (i.e., those exceeding half of the highest frequency), and half-band high-pass filter removes all frequencies that are below half of the highest frequency [25–27].
(2) The convolution outputs are down-sampled by two, The mathematics of convolution operation are

$$x[n] * h[n] = \sum_{k=-\infty}^{\infty} x[k]h[n-k] \tag{1}$$

Hence, the outputs of the down-sampling operation will have only half of the number of the samples. After the down-sampling operation, the scale of the signal is twice the original signal scale [25–27]. The output of first level

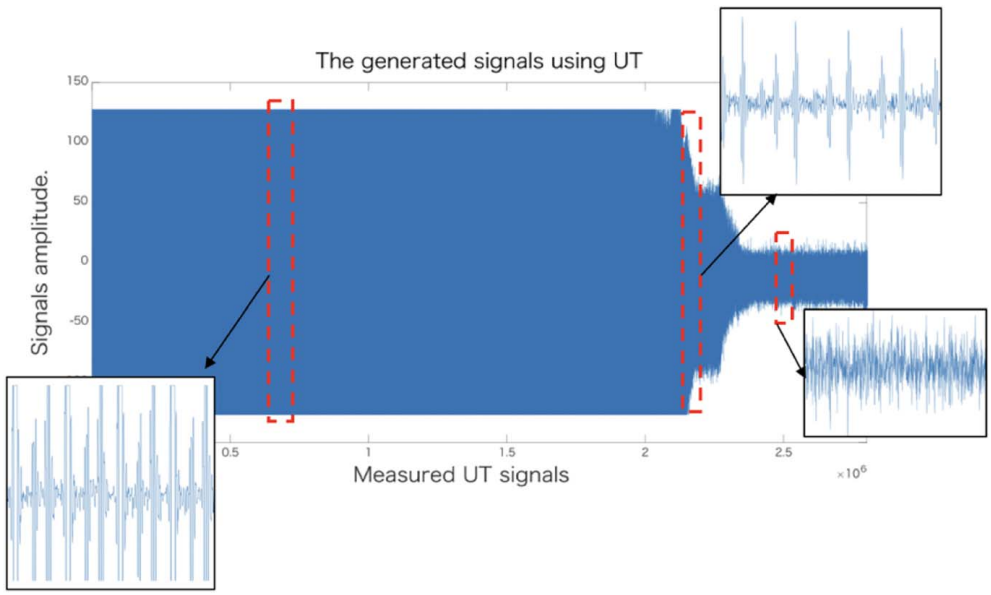

Fig. 9 Measurements of UT signal for a completed experiment, and (from left to right) red dashed lines showing the location of a normal UT signal, attenuated UT signal, and noisy signal, respectively (Color version online.)

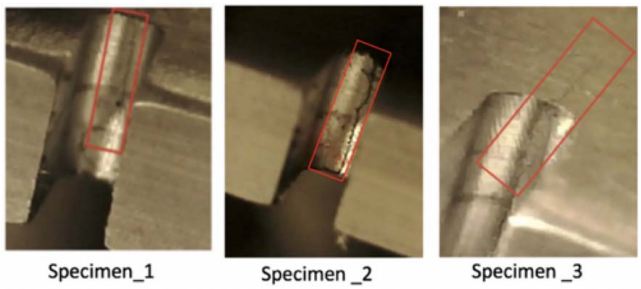

Fig. 10 Microscope images for VT of fatigue cracks

decomposition is expressed as

$$y_{lo}[k] = \sum_n x[k]h[2n-k]$$

$$y_{hi}[k] = \sum_n x[k]\ g[2n-k]$$

where y_{lo} and y_{hi} represent the outputs of the low-pass and high-pass filters, respectively, after down-sampling by 2.

From the procedure of the first stage, called analysis filter, for the first level of the decomposition, we observe that the signal is decomposed into a coarse (or approximation) signal, $y_{lo}[k]$, and detail signal, $y_{hi}[k]$, by analyzing the signal at different frequency bands with different resolutions. The DWT function that is associated with a low-pass filter is defined as the scaling function, ϕ, as shown in Fig. 5(*a*). On the other hand, Fig. 5(*b*) represents the wavelet function, ψ, which is associated with high-pass filter. According to Nyquist's rule, which says that after filtering operation half the samples can be removed, the signal is down-sampled by two without losing any signal information, because half of the number of the samples are redundant. The signal decomposition of the first level reduces the time-resolution by 50% because only 50% of the samples represents the whole signal. The frequency resolution is doubled since the signal frequency band extends only half the prior frequency band. In this paper, this analysis procedure is repeated for the next level, until level four. The low-pass filter and high-pass filter satisfy the property of quadrature mirror filters [26,27], where the relationship between the impulse responses of both filters is related to each other by $g[M-1-n] = (-1)^n\ h[n]$, where M is the filter length, $g[n]$ is the high-pass filter, and $h[n]$ is the low-pass filter.

The second stage of DWT is called the synthesis filter bank [26]. The procedure of the second stage is as follows:

(1) The outputs at every level from the analysis filter bank are up-sampled by two.
(2) The outputs of the up-sampling operation pass through a half-band digital filters (low-pass or high-pass).
(3) The outputs of the high-pass filter and low-pass filter are combined to construct the input of the next level of the synthesis filter bank.

From the above procedure, we observe the following:

- The procedure order of the synthesis filter bank is a mirror of the analysis filter bank procedure.
- The first stage and the second stage of DWT are analogous to each other, excluding a time reversal.
- The orthonormal bases of half-band filters assist the signal to be reconstructed. Thus, a condition of the signal reconstruction is half-band filtering.

The signal reconstruction for each level is obtained as

$$x[n] = \sum_{k=-\infty}^{\infty} ((y_{lo}[k]\ h[-n+2k]) + (y_{hi}[k]\ g[-n+2k])) \qquad (2)$$

4.2 The Hilbert Transform. HT is one of the fundamental operators in the field of signal processing, which was introduced by David Hilbert to solve a special case of the Riemann–Hilbert problem [17,28]. The HT of a signal $x(t)$, represented as $\hat{x}(t)$, is

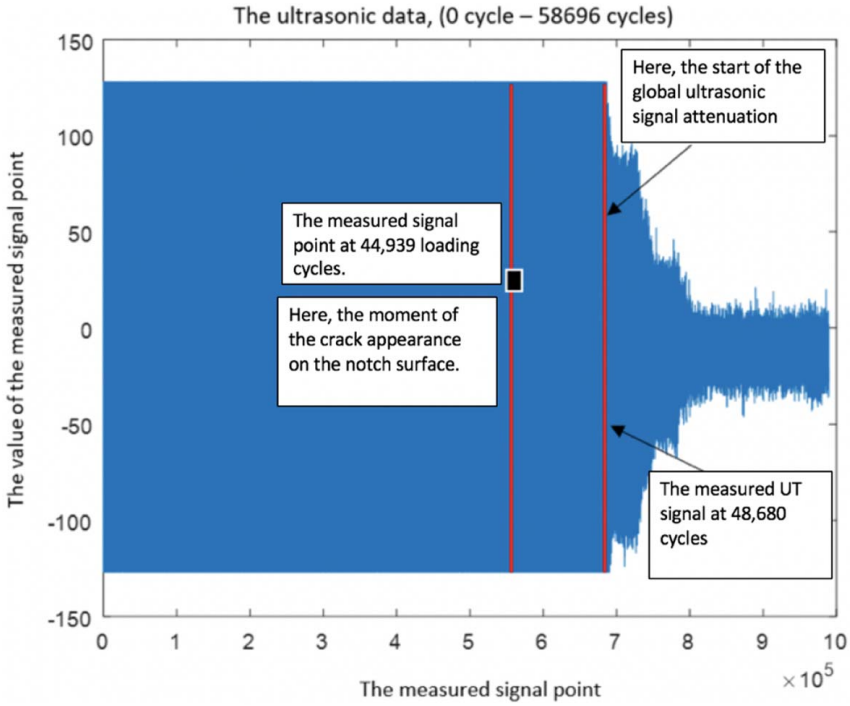

Fig. 11 Measured ultrasonic signals for specimen 1: (from left to right) the first red dashed line representing the location of VT crack detection and the second red dashed line representing typical UT crack detection (Color version online.)

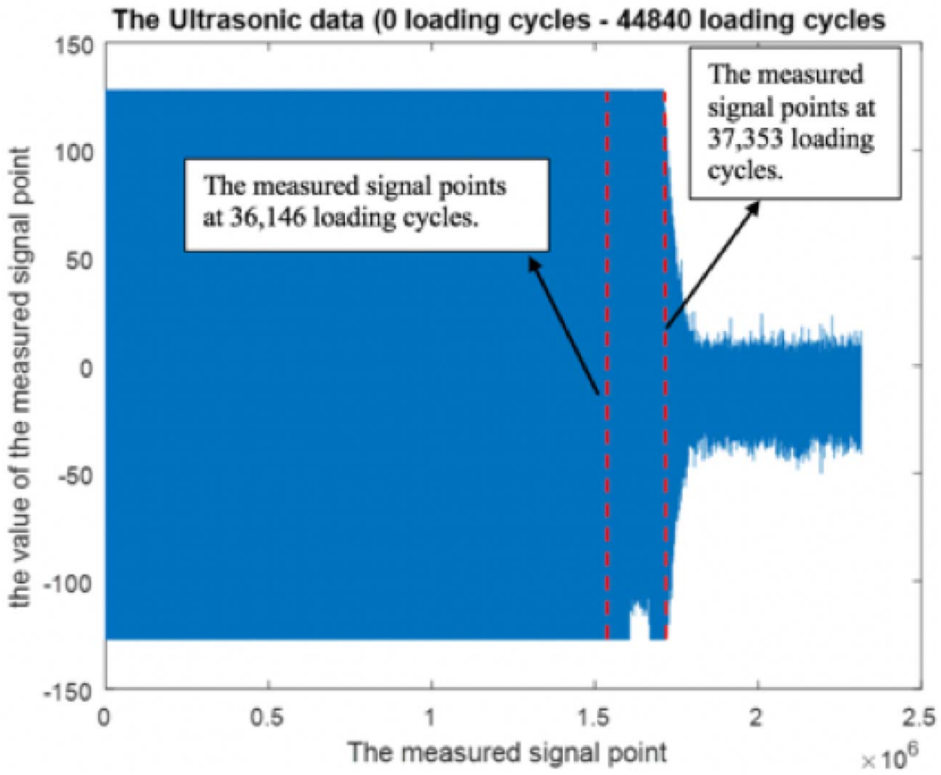

Fig. 12 Measured ultrasonic signals for specimen 2: (from left to right) the first red dashed line representing the location of VT crack detection and the second red dashed line representing typical UT crack detection (Color version online.)

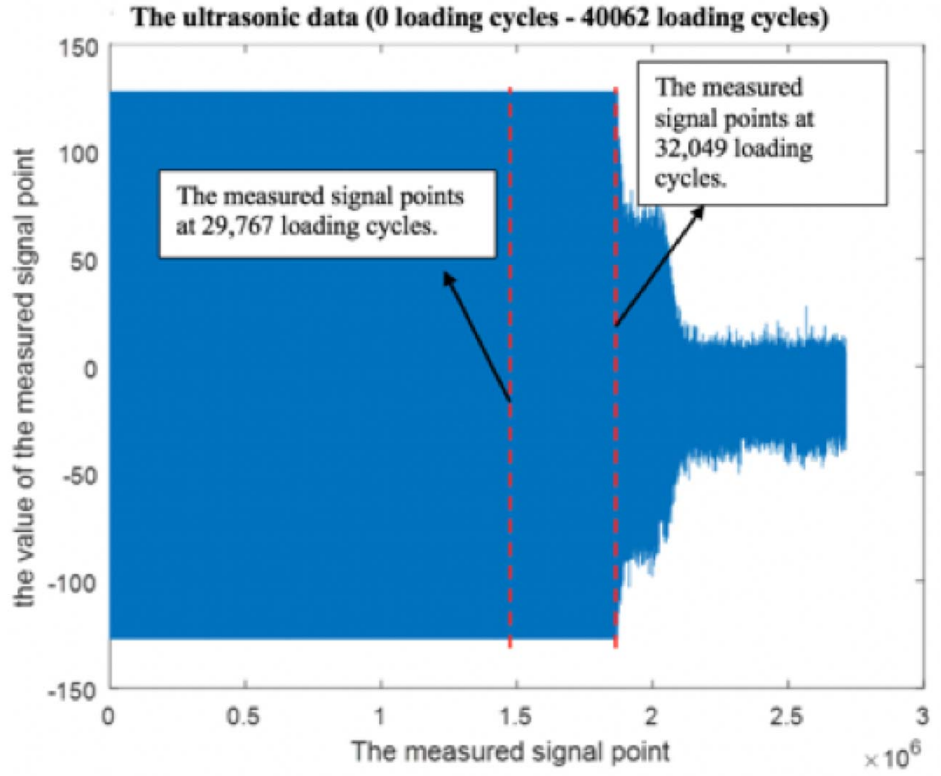

Fig. 13 Measured ultrasonic signals for specimen 3: (from left to right) the first red dashed line representing the location of VT crack detection and the second red dashed line representing typical UT crack detection (Color version online.)

Table 1 Instants of the fatigue crack detection using VT and UT

	VT detection (loading cycles)	UT detection (loading cycles)	UT delay (loading cycles)	No. of measured points using UT
Specimen 1	44,939	8680	3741	$0.99 * 10^6$
Specimen 2	36,146	37,353	1207	$2.3 * 10^6$
Specimen 3	29,767	32,049	2282	$2.7 * 10^6$

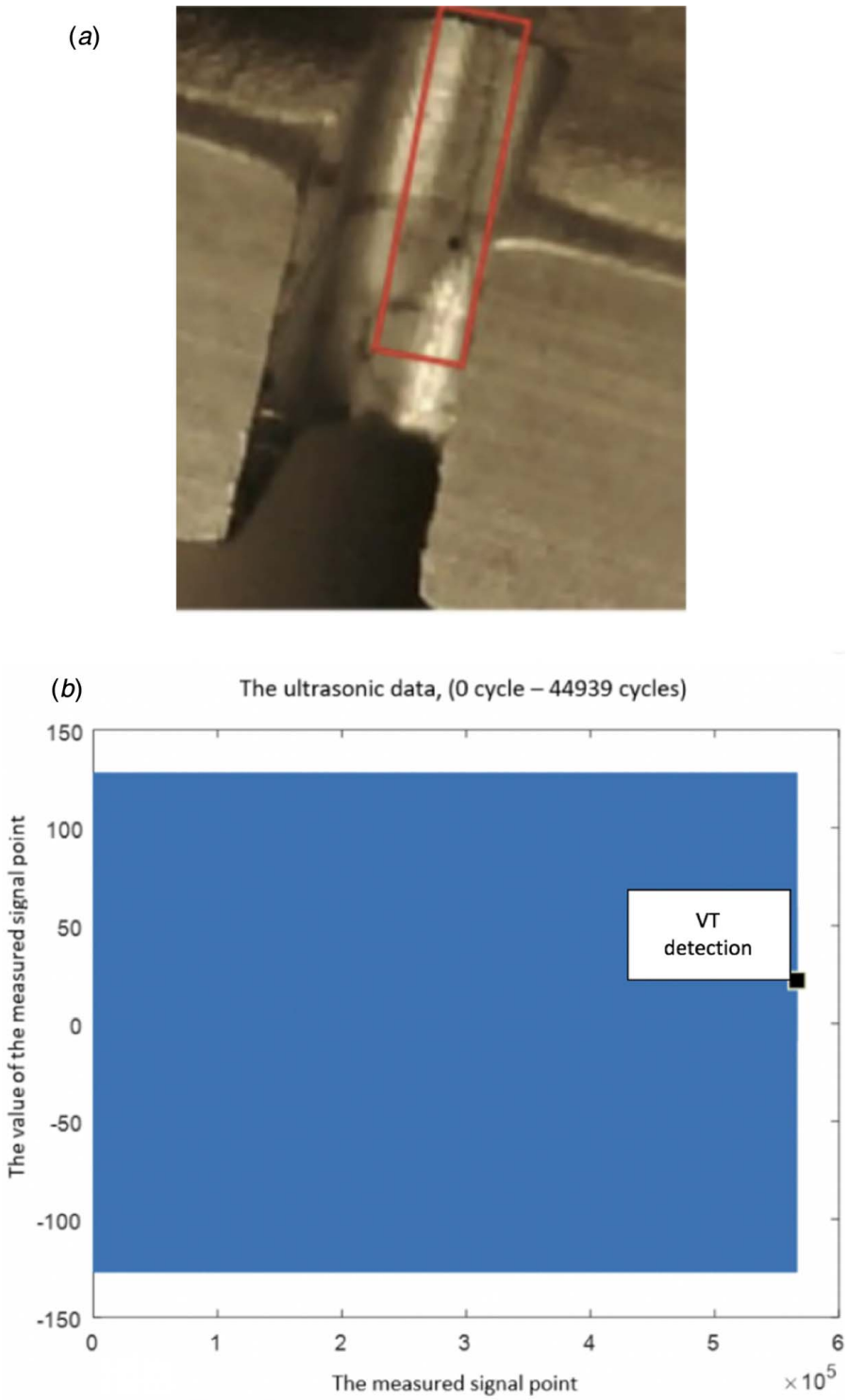

Fig. 14 Crack detection using VT image and UT data for specimen 1: UT data include UT signal measurements from beginning of the experiment until VT crack detection, where the end of UT data denotes the location of VT detection: (*a*) reference detection (VT image) and (*b*) corresponding UT data for crack detection

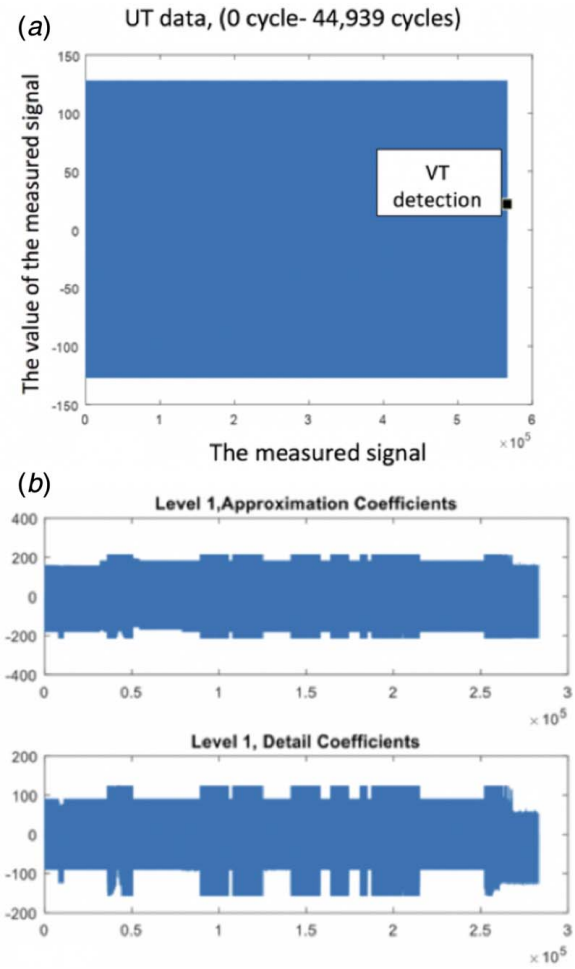

Fig. 15 Signal decomposition at level-1 of MRA: (*a*) the measured points of the ultrasonic signals, from 0 cycle to 44,939 loading cycles and (*b*) first level of the approximation coefficients and detail coefficients of DWT

computed via the following integral:

$$\hat{x}(t) = \frac{1}{\pi}\int_{-\infty}^{\infty} \frac{x(\tau)}{(t-\tau)}\,\mathrm{d}\tau \tag{3}$$

The key points of HT are as follows:

(1) The HT does not involve a change in signal domain. However, the HT output $\hat{x}(t)$ is different from the original signal $x(t)$.
(2) The HT shifts the angle phase of the original signal $x(t)$ by $-\pi/2$ radians without changing its amplitude as seen in the following example:
- Example 1: The HT for a signal $x(t) = \cos(\omega t)$ is $\hat{x}(t) = \sin(\omega t)$.

(3) One method to construct $\hat{x}(t)$ is to multiply the positive spectrum (i.e., positive frequencies) of the continuous-time signal $x(t)$ by the $-\pi/2$ rotation operator $-j$ and the negative spectrum (i.e., negative frequencies) of $x(t)$ by the $+\pi/2$ rotation operator $+j$, and the output is HT in the frequency domain which is also the FT $\mathcal{F}[\hat{x}(t)]$. Then, by taking the inverse Fourier transform (IFT) $\mathcal{F}^{-1}$, the HT of the signal $\hat{x}(t)$ can be obtained by the convolution of $x(t)$ with the HT kernel $h(t)$ as seen as follows:

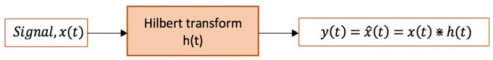

$$y(t) = \hat{x}(t) = \int_{-\infty}^{\infty} x(\tau)\, h(t-\tau)\,\mathrm{d}\tau \tag{4}$$

Thus, the FT of $y(t)$ is

$$Y(\omega) = \mathcal{F}[\hat{x}(t)] = X(\omega)\; H(\omega) \tag{5}$$

By applying IFT $\mathcal{F}^{-1}$ on Eq. (5), we reconstruct $\hat{x}(t)$ as

$$\hat{x}(t) = \mathcal{F}^{-1}\Big(X(\omega)\; H(\omega)\Big) \tag{6}$$

Now, we define the function $H(\omega)$ such that

$$H(\omega) = \begin{cases} -j, & \omega > 0 \\ j, & \omega < 0 \end{cases} \tag{7}$$

$$\text{i.e.,} \quad H(\omega) = -j\ \mathrm{sign}(\omega)$$

Then, the IFT $\mathcal{F}^{-1}[H(\omega)]$ is

$$h(t) = \frac{1}{\pi t} \tag{8}$$

By substituting Eq. (8) into Eq. (4), HT of a signal $x(t)$ is defined, as illustrated in Eq. (3).

4.3 Properties of Hilbert Transform. The salient properties of HT are summarized as follows:

(1) The HT of an even signal is odd, and the HT of an odd signal is even. Specifically, the HT of $\hat{x}(t)$ is $-x(t)$, i.e., $\hat{\hat{x}}(t) = -x(t)$, as seen in the following example:
- If $x(t) = \cos(t)$, then the HT is $\hat{x}(t)$ (see Example 1). Then, its HT is

$$\hat{\hat{x}}(t) = \sin(\omega t - \pi/2) \;\Rightarrow\; \hat{\hat{x}}(t) = -x(t) \tag{9}$$

(2) The signal $x(t)$ and its HT $\hat{x}(t)$ are mutually orthogonal, i.e.,

$$\int_{-\infty}^{\infty} x(t)\;\hat{x}(t) = 0 \tag{10}$$

(3) The energy of a signal $x(t)$ is identically equal to that of its HT $\hat{x}(t)$, i.e.,

$$\int_{-\infty}^{\infty} |x(t)|^2\, dt = \int_{-\infty}^{\infty} |\hat{x}(t)|^2\, dt \tag{11}$$

As stated in Sec. 1, the main objective of using HT in this paper is to apply the envelope detection method on the UT data. The envelope of the original time-domain signal is obtained directly from the magnitude of the analytical signal which is defined as

$$a(t) \triangleq x(t) + j\hat{x}(t) \tag{12}$$

where $x(t)$ is a typical UT signal and $\hat{x}(t)$ is its HT. Then, the signal envelope of $x(t)$ is defined as

$$\mathrm{env}_x(t) \triangleq \sqrt{|x(t)|^2 + |\hat{x}(t)|^2} \tag{13}$$

An example follows:

- Example 2: Let us create a time-domain signal $x(t)$ that decays over time so that we can observe how the envelope characterizes the decay (note: the decay parameter $\lambda > 0$):

$$x(t) = A\;\exp(-\lambda\; t)\;\sin(\alpha\; t) \tag{14}$$

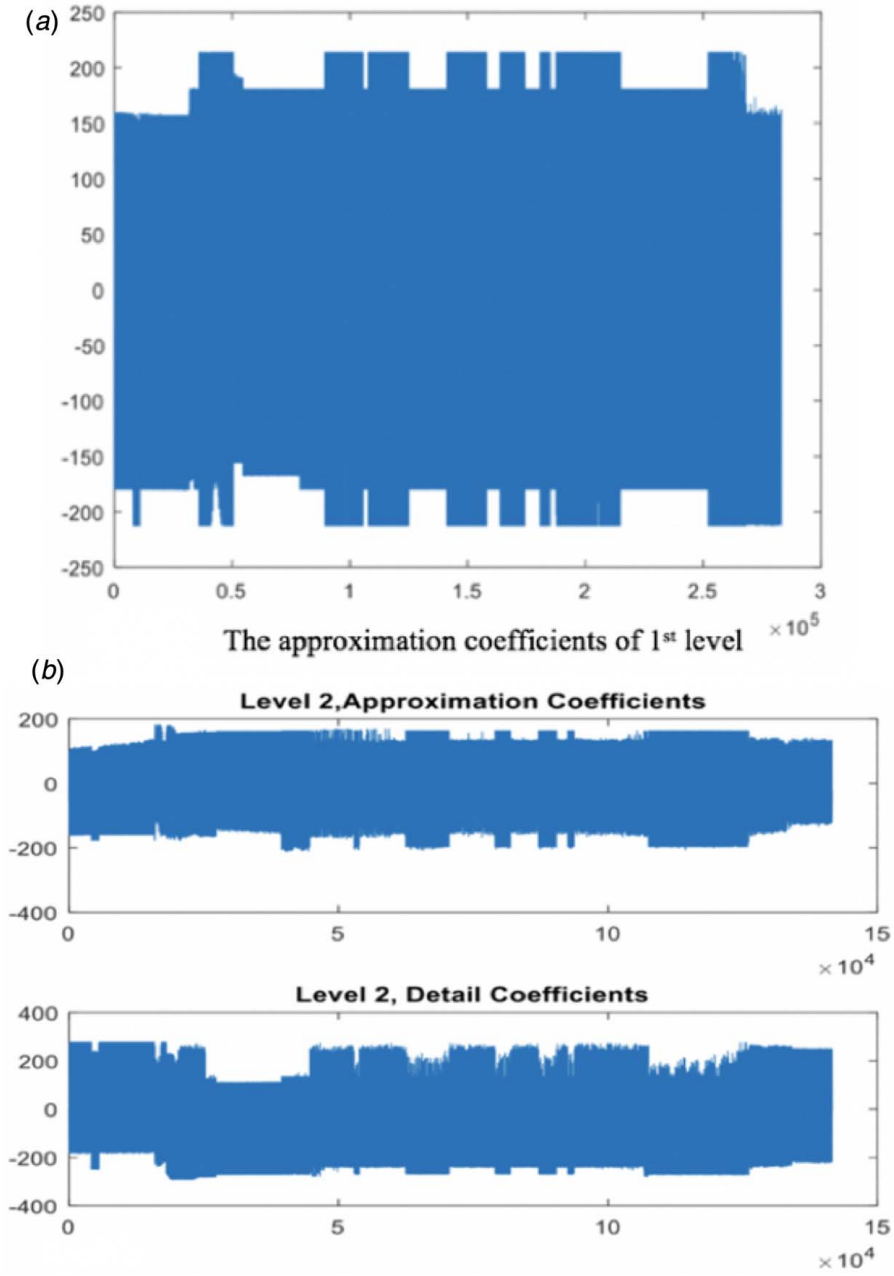

Fig. 16 Signal decomposition at level-2 of MRA: (*a*) approximation signal at level-1 as input to level-2 and (*b*) approximation and detail coefficients at level-2

and its HT is

$$\hat{x}(t) = A \ \exp(-\lambda \ t) \ \cos(\alpha \ t) \tag{15}$$

Figures 8(*a*) and 8(*b*) present the original signal and its HT signal, respectively. It follows from Fig. 8(*c*) that the envelope detection method using HT provides a perfect characterization for identification of the decay rate of the signal $x(t)$.

Now we show how to detect the fatigue crack onset using the information on energy of the UT signal. Figure 9 shows that the UT signal in a typical test specimen starts as stable and remains (nearly) constant until the onset of the fatigue crack. Then, it starts to decay, because part of the signal is reflected back to its source due to the increase in ultrasonic impedance resulting from the fatigue damage initiation. Consequently, envelope detection (see Eq. (13)) becomes applicable for detection of the signal attenuation in the UT signal.

4.4 Analysis of Ultrasonic Testing Signals Via Discrete Wavelet Transform and Hilbert Transform. The proposed procedure of fatigue damage detection, which is a synergistic combination of DWT and HT and also makes use of VT data, is briefly described in the following steps as:

(1) Determine the energy of each UT signal over its entire range (see Eq. (11)).
(2) Determine the envelope of each UT signal energy over its entire range (see Eq. (13)).
(3) Identify the instant when the reduction in the envelope of UT signal energy initiates by applying DWT on the envelope of UT signal energy—this is the onset of fatigue crack damage.

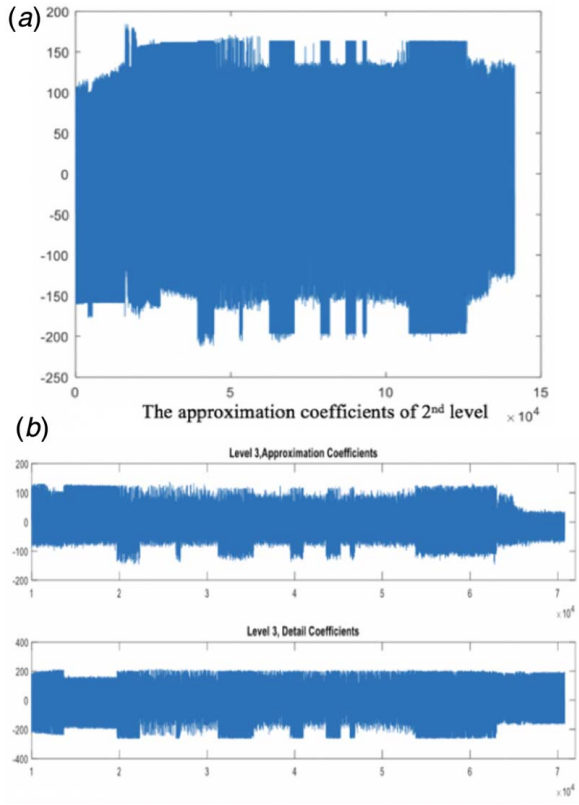

Fig. 17 Signal decomposition at level-3 of MRA: (*a*) approximation signal at level-2 as input to level-3 and (*b*) approximation and detail coefficients at level-3

(4) Compare the result for the proposed method with those of other methods such as DWT, HT, and VT.

As illustrated in the analysis procedure, the proposed detection method takes advantage of both HT and DWT, where HT characterizes the envelope of UT signal energy, and DWT determines the instant of crack onset by analyzing the envelope of UT signal energy at different scales and time translations.

5 Results and Discussion

This section presents and discusses the results of experiments pertaining to detection of fatigue crack onset in polycrystalline alloy (i.e., AL7075-T6) specimens using both VT and UT data. The results of UT data analysis can be obtained by both DWT and HT individually; in this paper, the results of the proposed method (i.e., a combination of DWT and HT) have been compared with those of the individual methods (i.e., DWT and HT) by having VT images of fatigue crack as the ground truth, which were generated by the digital microscope.

5.1 The Ultrasonic Testing Data Analysis Using Discrete Wavelet Transform. As described in Sec. 2, UT data were generated synchronously with the images obtained from the digital microscope. Figure 10 presents images of fatigue cracks on the curved surface inside the notch of test specimens. However, a casual inspection of UT data (e.g., see Fig. 9) does not provide any additional information beyond VT data that serve as the ground truth for crack detection. This issue is further explained below.

Figures 11–13 show profiles of UT data for specimen 1, specimen 2, and specimen 3, where it is seen by visual inspection that fatigue crack onsets occur at ~48,680, ~37,353, and ~32,049 loading cycles, respectively. Table 1 shows the loading cycles

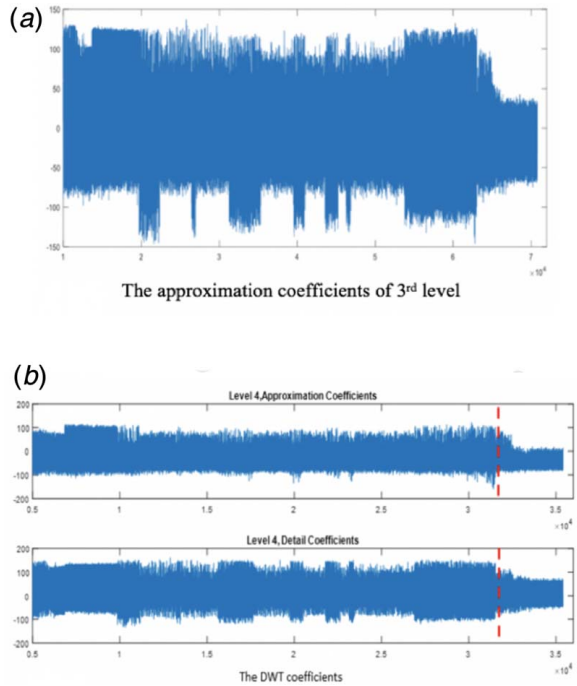

Fig. 18 Signal decomposition at level-4 of MRA: (*a*) approximation signal at level-3 as input to level-4 and (*b*) approximation and detail coefficients at level-3 (Color version online.)

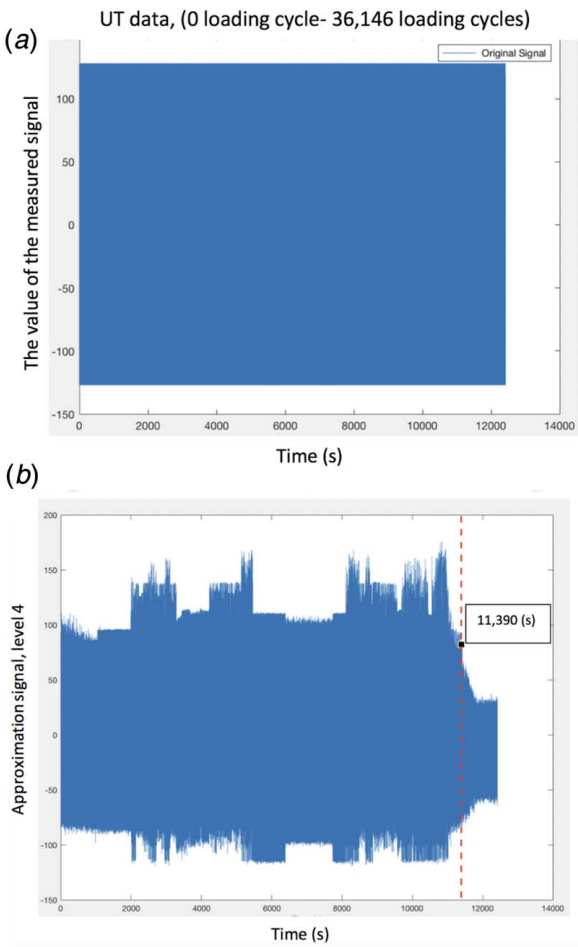

Fig. 19 MRA detection at level-4 for specimen 2: (*a*) UT signals (0 to 36,146) loading cycles and (*b*) corresponding level-4 approximation

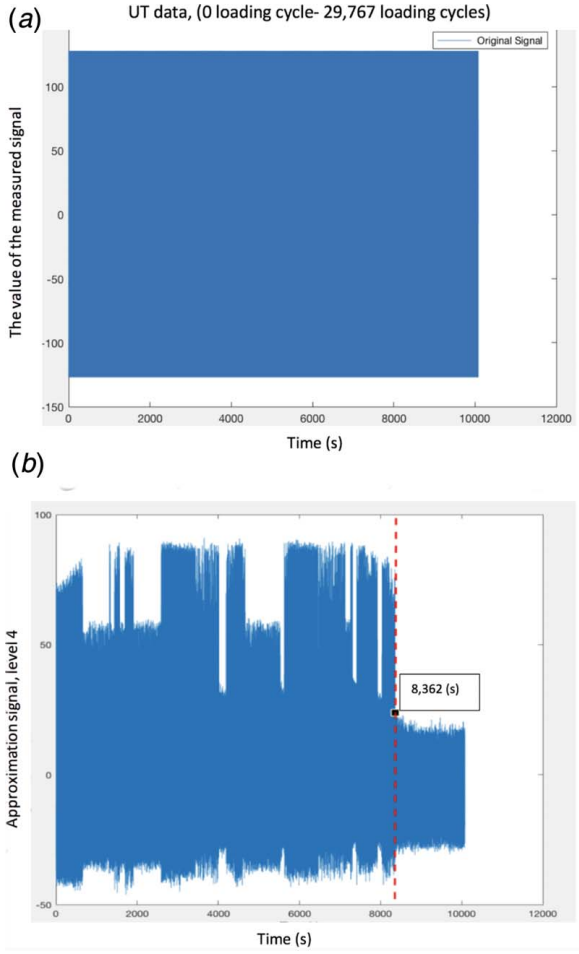

Fig. 20 MRA detection at level-4 for specimen 3: (*a*) UT signals (0 to 29,767) loading cycles and (*b*) corresponding level-4 approximation

observed from both VT images and UT data at the crack onset for these three specimens along with delay of UT data and the amount of measured data. It is noted that VT images consistently detect cracks earlier than casual inspection of UT data. In other words, a casual inspection of UT data provides the information on crack detection after the crack is propagated, *not* before or at the beginning of crack propagation. Therefore, *a rigorous analysis of UT data is necessary to provide useful information on a forthcoming crack before the VT images do*. In this process, the collection of UT data may start anytime after the beginning of the experiment but not after the instant of crack detection by VT.

One of the methods that is capable of generating the above information from UT data is DWT. Following the block diagram in Fig. 7, the procedure for DWT-based analysis of UT data for crack detection (e.g., for specimen 1 in Fig. 14) is described in the following steps:

Table 2 Instants of fatigue crack detection using VT and DWT on UT

	VT detection (min)	UT detection using DWT (min)	DWT detection performance improvement (min)
Specimen 1	259	233	26
Specimen 2	207	185.33	21.67
Specimen 3	168	139.36	28.64

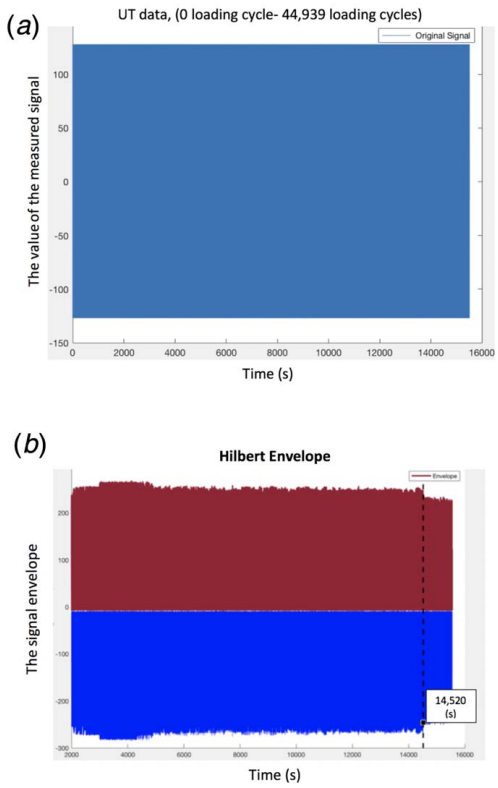

Fig. 21 HT detection for specimen 1: (*a*) UT signals (0 to 44,939) loading cycles and (*b*) corresponding Hilbert envelope

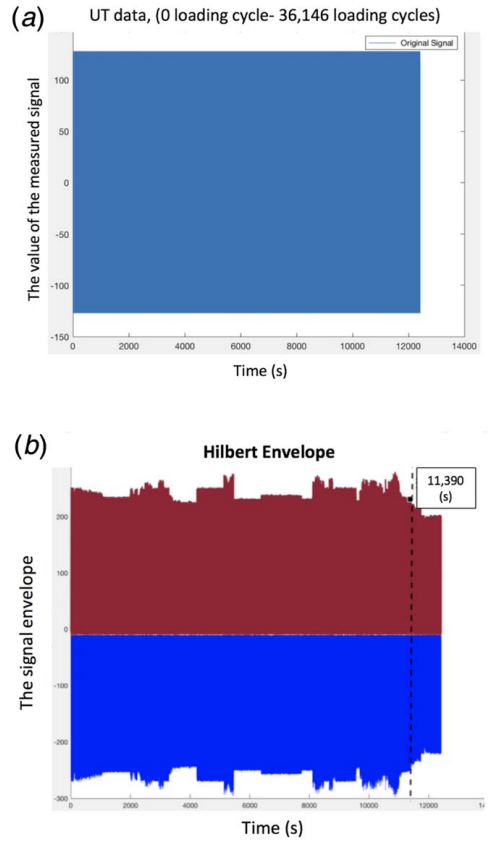

Fig. 22 HT detection for specimen 2: (*a*) UT signals (0 to 36,146) loading cycles and (*b*) corresponding Hilbert envelope

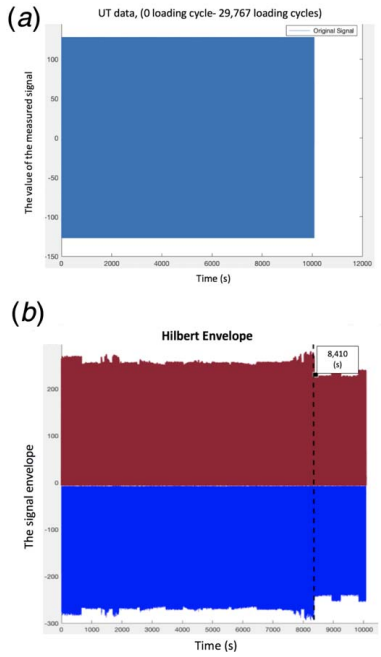

Fig. 23 HT detection for specimen 3: (*a*) UT signals (0 to 29,767) loading cycles and (*b*) corresponding Hilbert envelope

(1) The original signal $s(n)$ is obtained from UT data, which represents the measured signal points from the beginning of the experiment until the VT detection that serves as the ground truth, as seen in Fig. 15(*a*).
(2) The input to the first level DWT is the original signal which is decomposed into approximation output $y_{lo}[k]$ and detail output $y_{hi}[k]$, as seen in Fig. 15(*b*).

Table 3 Instants of fatigue crack detection using VT and HT on UT

	VT detection (min)	UT detection using HT (min)	HT detection performance improvement (min)
Specimen 1	259	242	17
Specimen 2	207	189.83	17.17
Specimen 3	168	140.16	27.84

(3) The first level of the approximation output $y_{lo}[k]$ becomes the input signal at the second level of the analysis filter bank for decomposition into new approximation and detail outputs, as seen in Fig. 16.
(4) This process of signal decomposition is continued to the third level and fourth level of the analysis filter banks, where the input signal of each level is the approximation output of the previous level. In other words, the input signal at each level is decomposed into new approximation and detail outputs as seen in Figs. 17 and 18.

For specimen 1, decomposition of UT signals at the fourth level shows clear trends of decay in both approximation and detail coefficients as shown by the vertical red dashed lines in two plots of Fig. 18(*b*); this forecasts the onset of fatigue crack. Similar incidents are also seen in Figs. 19(*b*) and 20(*b*) for fatigue crack detection for both specimen 2 and specimen 3. Thus, the consistency of results from three test specimens evinces that wavelet decomposition of ultrasonic signals by DWT analysis provides pertinent information for forecasting and detection of fatigue crack onset.

Determination of the onset time of a fatigue crack from VT images is required, because it serves as the reference point for evaluation of the prediction capability of the DWT-based and other methods. The reference detection time is measured from the experiment startup until the appearance of the fatigue crack on the notch

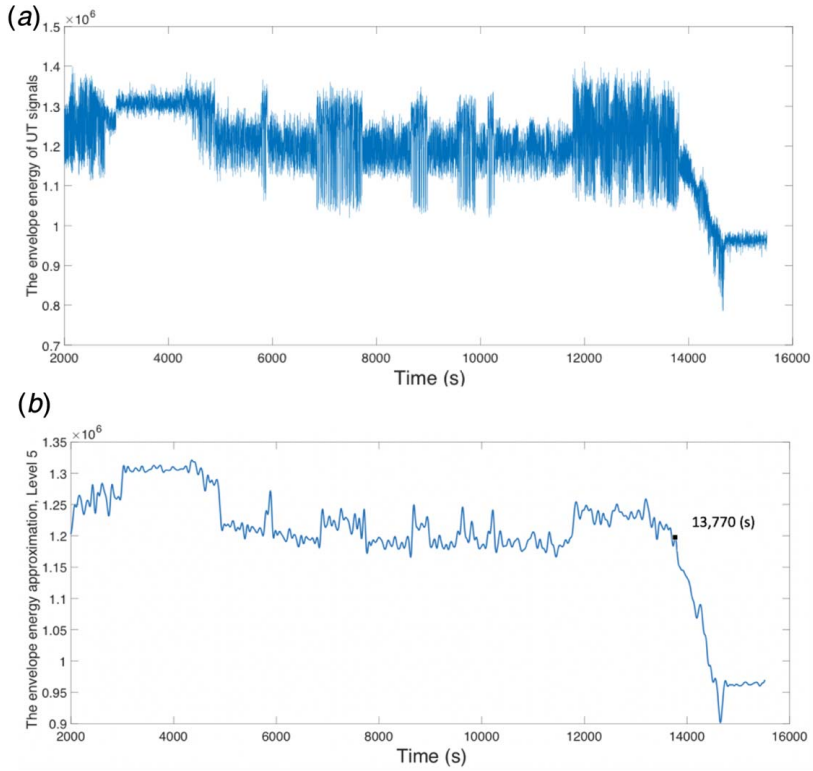

Fig. 24 Detection by the proposed method for specimen 1: (*a*) Hilbert envelope of UT signal energy (0 to 44,939) loading cycles and (*b*) corresponding approximation of signal energy envelope at level-5

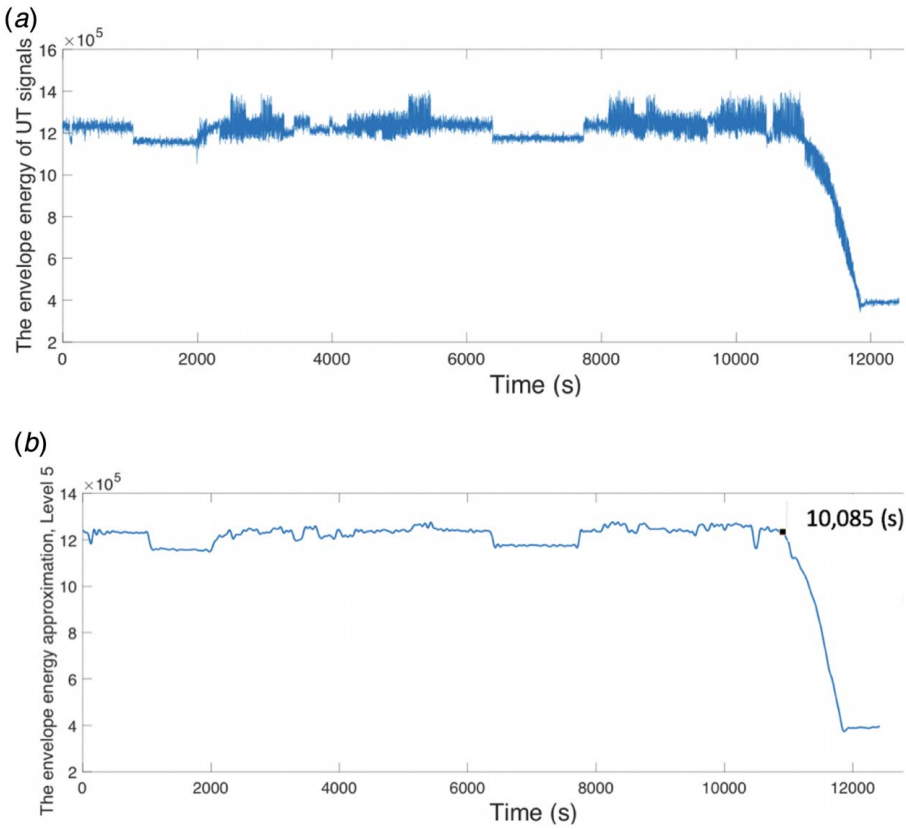

Fig. 25 Detection by the proposed method for specimen 2: (*a*) Hilbert envelope of UT signal energy (0 to 36,146) loading cycles and (*b*) corresponding approximation of signal energy envelope at level-5

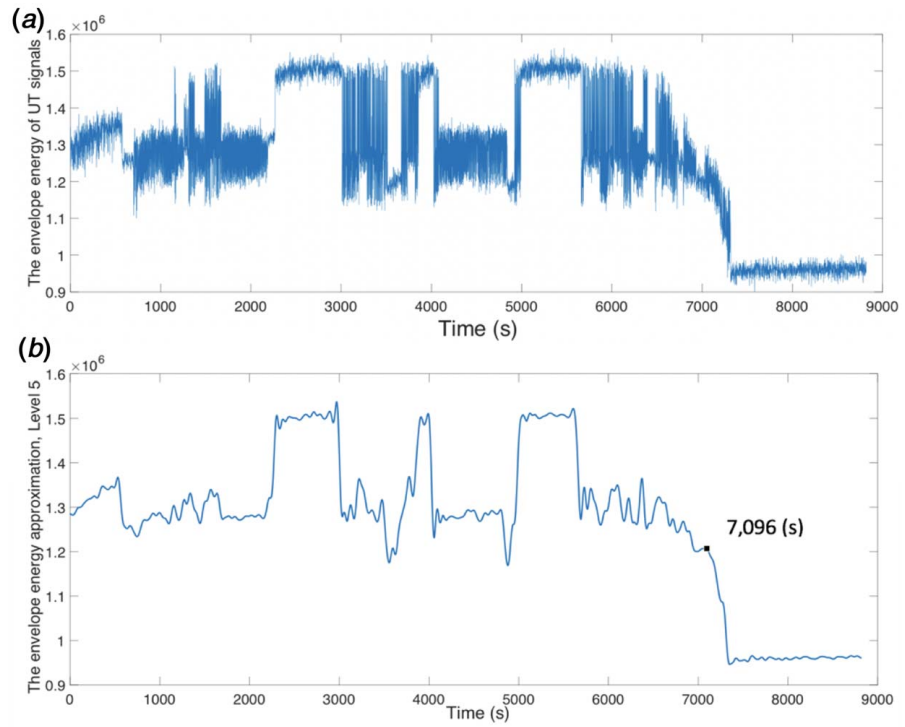

Fig. 26 Detection by the proposed method for specimen 3: (*a*) Hilbert envelope of UT signal energy (0 to 29,767) loading cycles and (*b*) corresponding approximation of signal energy envelope at level-5

Table 4 Instants of fatigue crack detection using VT and the proposed method

	VT detection (min)	The proposed method detection (min)	The proposed detection performance improvement (min)
Specimen 1	259	229.5	29.5
Specimen 2	207	180.8	26.16
Specimen 3	168	118.5	49.5

Table 5 Data size of UT signal envelope and UT signal energy envelope

	The size of UT data (number of measured points)	The size of our method data (number of measured points)
Specimen 1	1,590,086	10,891
Specimen 2	1,535,779	9539
Specimen 3	895,763	7403

surface (i.e., VT detection time). As seen in Table 2, the DWT-based detection yields a significant improvement in forecasting of fatigue crack onset as compared to VT detection.

5.2 Analysis of Ultrasonic Testing Data by Hilbert Transform. Following Sec. 4.2, the signal envelope after HT characterizes the shape of the upper and the lower boundaries of UT signals. As a part of the ultrasonic signal is reflected back to the source due to a fatigue crack, both upper and the lower boundaries of the signal are changed. Figures 21–23 present detection of fatigue crack onset for specimen 1, specimen 2, and specimen 3, respectively, using HT-based envelope detection, where the fatigue crack onset is forecast in advance of detection by the respective VT images, as indicated by vertical dashed lines. As seen in Table 3, the HT-based detection yields an improvement in forecasting of fatigue crack onset as compared to VT detection. A comparison of Tables 2 and 3 reveals that although both DWT and HT are capable of forecasting fatigue cracks in advance of the VT-based detection, DWT is consistently superior to HT; however, the computational complexity of DWT-based forecasting (requiring eight analytical operation cycles) is considerably higher than that of HT (requiring two analytical operation cycles).

5.3 Proposed Method of Ultrasonic Testing Data Analysis. The proposed method provides good performance for fatigue crack forecasting and detection with reduced computational complexity. Thus, DWT is a desirable application on data analysis for performance improvement while the computational complexity is reduced with mitigated data analysis by the usage of signal energy envelope instead of signal envelope samples. Figures 24–26 illustrate the fatigue crack onset detection using the HT-based envelope of UT signal energy and then applying DWT. As shown in Figs. 24(*a*), 25(*a*), and 26(*a*), the usage of signal energy envelope improves the fatigue crack forecasting almost similar to what has been achieved by DWT and HT. Furthermore, the signal energy envelope is analyzed using DWT, both locally and globally, which yields superior performance, as shown in Figs. 24(*b*), 25(*b*), and 26(*b*). Table 4 presents the detection performance using the proposed method, where the results are compared with those of VT for three specimens. The proposed method is capable of forecasting an incipient fatigue crack well ahead of VT (i.e., using digital microscope); therefore, a forthcoming crack could be detected in its initiation regime (i.e., before reaching the propagation propagation regime).

Fig. 27 Comparison study for the moment of the crack detection methods and the improvement of detection performance: (*a*) instants (min) of crack detection by four methods and (*b*) reduction in detection time of DWT, HT, and the proposed method as compared to VT

The proposed method also has a significant advantage toward reduction of computational complexity as compared to conventional DWT, because the data size of signal energy envelope, to be analyzed in the proposed method, is significantly less than that of the original UT data by DWT. Table 5 lists the difference in the data size between the proposed method and the original UT data, where the amounts of analyzed are significantly reduced to 6.84%, 6.2%, and 8.3% of the original UT data for specimen 1, specimen 2, and specimen 3, respectively. Figure 27(*a*) compares the instants in minutes of fatigue crack detection for all tested methods, and Fig. 27(*b*) shows the improvement in the fatigue crack forecasting time in minutes for all tested methods as compared to VT detection, which is treated as the ground truth for crack onset in this paper.

6 Summary, Conclusions, and Future Work

The research work reported in this paper has presented a methodology of real-time health monitoring to forecast and detect fatigue crack damage in mechanical structures using DWT and HT of available data. Two types of data sources have been used for real-time sensing of damage, which are based on (i) VT images from a digital microscope and (ii) UT data. While the digital microscope facilitates VT-based detection, its usage outside a laboratory environment is time-consuming and expensive. The underlying algorithm of the proposed method is built upon a synergistic combination of DWT and HT-based envelope detection, which takes advantage of the attenuation of UT signal energy at the

onset of fatigue crack. The proposed method requires much less data than the conventional DWT, and its computational complexity is significantly reduced relative to DWT.

It is concluded that, compared to conventional DWT, the proposed method of fatigue crack forecasting and detection not only yields better performance but also is computationally much less complex. While there are many areas of both theoretical and experimental research that should be undertaken before its commercial application, the following topics are suggested by the authors for future research:

(1) Examination of the detailed information at different levels of DWT.
(2) Investigation of signal contents at different stages in the crack initiation regime.
(3) Image analysis by more advanced apparatuses of optical metrology (e.g., confocal microscopy).

Acknowledgment

The first author gratefully acknowledges the financial support of the Saudi Arabian Cultural Mission (SACM). The work reported in this paper has been supported in part by U.S. Air Force Office of Scientific Research (AFOSR) under grant no. FA9550-15-1-0400.

Conflict of Interest

There are no conflicts of interest.

References

[1] Ohring, M., and Kasprzak, L., 1998, Chapter 9-Degradation of Contacts and Package Interconnections, M. Ohring, ed., Academic Press, Cambridge, MA, pp. 475–537.
[2] Hopkins, P., 2003, "The Structural Integrity of Oil and Gas Transmission Pipelines," Comprehensive Struct. Int., **1**, pp. 87–123.
[3] Wong, W., 2010, "Asset Integrity: Learning About the Cause and Symptoms of Age and Decay and the Need for Maintenance to Avoid Catastrophic Failures," Risk Manage. Safety Dependability, pp. 188–225.
[4] Ray, A., and Patankar, R., 2001, "Fatigue Crack Growth Under Variable-Amplitude Loading: Part I—Model Formulation in State-Space Setting," Appl. Math. Model., **25**(11), pp. 979–994.
[5] Ray, A., and Patankar, R., 2001, "Fatigue Crack Growth Under Variable-Amplitude Loading: Part II—Code Development and Model Validation," Appl. Math. Model., **25**(11), pp. 995–1013.
[6] Cawley, P., 2001, "Non-destructive Testing—Current Capabilities and Future Directions," Proc. I MECH E Part L J. Mater.:Des. Appl., **215**(4), pp. 213–223.
[7] Gholizadeh, S., 2016, "A Review of Non-destructive Testing Methods of Composite Materials," Proc. Struct. Integrity, **1**, pp. 50–57.
[8] Singh, R., 2016, "Ultrasonic Testing," Appl. Weld. Eng., pp. 343–355.
[9] Campbell, F. C., 2013, *Inspection of Metals: Understanding the Basics*, ASM International, Materials Park, OH.
[10] Birks, A. S., Greene, R. E., and Moore, P., 1991, *Nondestructive Testing Handbook, Vol. 7. Ultrasonic Testing*, American Society for Nondestructive Testing, Columbus, OH.
[11] Garnier, C., Pastor, M.-L., Eyma, F., and Lorrain, B., 2011, "The Detection of Aeronautical Defects In Situ on Composite Structures Using Non Destructive Testing," Compos. Struct., **93**(5), pp. 1328–1336.
[12] Shull, P. J., 2002, *Nondestructive Evaluation: Theory, Techniques, and Applications*, CRC Press, Boca Raton, FL.
[13] Kaiser, G., 1994, *A Friendly Guide to Wavelets*, Birkhauser, Boston, MA.
[14] Mallat, S., 2009, *A Wavelet Tour of Signal Processing: The Sparse Way*, 3rd ed., Academic Publishers, Amsterdam.
[15] Yu, D., Cheng, J., and Yang, Y., 2005, "Application of Emd Method and Hilbert Spectrum to the Fault Diagnosis of Roller Bearings," Mech. Syst. Signal Process., **19**(2), pp. 259–270.
[16] Fan, X., and Zuo, M. J., 2006, "Gearbox Fault Detection Using Hilbert and Wavelet Packet Transform," Mech. Syst. Signal Process., **20**(4), pp. 966–982.
[17] Klingspor, M., 2015, *Hilbert Transform: Mathematical Theory and Applications to Signal processing*, DiVA Linköping University, Linköping.
[18] Yang, Y., 2017, "A Signal Theoretic Approach for Envelope Analysis of Real-Valued Signals," IEEE Access, **5**, pp. 5623–5630. .
[19] Feldman, M., 2011, "Hilbert Transform in Vibration Analysis," Mech. Syst. Signal Process., **25**(3), pp. 735–802.
[20] Daubechies, I., 1992, *Ten Lectures on Wavelets*, SIAM Publishers, Philadelphia, PA.
[21] Debnath, L., and Shah, F. A., 2015, *Wavelet Transforms and Their Applications*, Springer, Boston, MA.
[22] Sang, Y.-F., 2012, "A Practical Guide to Discrete Wavelet Decomposition of Hydrologic Time Series," Water Res. Manage., **26**(11), pp. 3345–3365.
[23] Goel, A., 2014, "Discrete Wavelet Transform (DWT) With Two Channel Filter Bank and Decoding in Image Texture Analysis," Int. J. Sci. Res., **3**(4), pp. 391–397.
[24] Lee, B., and Tarng, Y., 1999, "Application of the Discrete Wavelet Transform to the Monitoring of Tool Failure in End Milling Using the Spindle Motor Current," Int. J. Adv. Manuf. Technol., **15**(4), pp. 238–243.
[25] Alonso, G. A., Gutiérrez, J. M., Marty, J.-L., and Muñoz, R., 2011, *Implementation of the Discrete Wavelet Transform Used in the Calibration of the Enzymatic Biosensors*, Intechopen, London, UK, pp. 135–153.
[26] Olivier, R., and Vetterli, M., 1991, "Wavelets and Signal Processing," IEEE Sig. Process., **8**(4), pp. 14–38.
[27] Oliveira, M. O., and Bretas, A. S., 2009, "Application of Discrete Wavelet Transform for Differential Protection of Power Transformers," 2009 IEEE Bucharest PowerTech, Bucharest, Romania, June 28–July 2, pp. 1–8.
[28] Kschischang, F. R., 2006, "The Hilbert Transform," Univ. Toronto, **83**, p. 277.